JACS
JOURNAL OF THE AMERICAN CHEMICAL SOCIETY

Communication

pubs.acs.org/JACS

High Thermal Stability Solution-Processable Narrow-Band Gap Molecular Semiconductors

Xiaofeng Liu,[†] Ben B. Y. Hsu,[‡] Yanming Sun,[‡] Cheng-Kang Mai,[†] Alan J. Heeger,[†,‡] and Guillermo C. Bazan*[,†,§]

[†]Center for Polymers and Organic Solids and Department of Chemistry and Biochemistry and [‡]Department of Physics, University of California, Santa Barbara, California 93106, United States

[§]Center of Excellence for Advanced Materials Research (CEAMR), King Abdulaziz University, Jeddah 22254, Saudi Arabia

Supporting Information

ABSTRACT: A series of narrow-band gap conjugated molecules with specific fluorine substitution patterns has been synthesized in order to study the effect of fluorination on bulk thermal stability. As the number of fluorine substituents on the backbone increase, one finds more thermally robust bulk structures both under inert and ambient conditions as well as an increase in phase transition temperatures in the solid state. When integrated into field-effect transistor devices, the molecule with the highest degree of fluorination shows a hole mobility of 0.15 $cm^2/V{\cdot}s$ and a device thermal stability of >300 °C. Generally, the enhancement in thermal robustness of bulk organization and device performance correlates with the level of C−H for C−F substitution. These findings are relevant for the design of molecular semiconductors that can be introduced into optoelectronic devices to be operated under a wide range of conditions.

Fluorine for hydrogen exchange within the framework of organic molecules has an extensive historical precedent and has made an impact in various applications, ranging from pharmaceutical chemistry to materials science.[1] This structural modification is also of interest within the design of molecular and polymeric organic semiconductors for integration into devices such as field-effect transistors (FETs) or organic solar cells (OSCs).[2] The small size of fluorine atom is generally suitable for altering the energetics of molecular orbitals without introducing extraordinary steric demands.[3] Hydrogen for fluorine substitution can also positively impact bulk heterojunction (BHJ) morphological features as they relate for use in OSCs.[4]

Attention to the thermal stability of the semiconductor component in devices, a relevant consideration for long-term stability, has not received the attention dedicated to the optimization of device performance merits, such as charge carrier mobilities and solar power conversion efficiencies.[5] Thermal stability predominantly refers to the temperature at which materials show evidence of degradation (i.e., weight loss). For application in thin-film devices, however, one needs to also consider the stability of useful morphological characteristics.[6] Previous efforts have been put toward looking at bulk structure stability as a function of thermal treatment.[7] Of relevance is the study of fluorinated anthradithiophenes, where fluorination is believed to enhance material crystallization and thermal stability.[8] Although one would argue that most applications rarely need to meet with overtemperature conditions, it is worthwhile considering that roll-to-roll printing and sintering may require materials, especially organic counterparts, to sustain functional bulk structures against temperature variation; factors that could promote long-term durability of thin-film devices.[9]

An established "intermediate-sized" donor−acceptor (D−A) conjugated molecule has shown OSC performance in the range of 6−7% without the use of solvent additives and postdeposition treatments (e.g., thermal annealing).[10] Herein, we describe our study based on these analogous molecular frameworks except for replacing "N" by C−F (highlighted in red), because (1) it behaves electronically similar to "N" within the molecular backbone, and (2) it is generally more tolerant than "N" to interfacial perturbation, e.g., protonation by acidic interlayers. In particular, we compare four molecules in two groups (distinguished by two different molecular lengths) with various degrees of fluorination, i.e., **F5**, **F6**, **F7**, and **F8** (Chart 1). Variations between C−F and C−H allow us to examine exclusively the influence of molecular fluorination on material bulk properties. It is of interest to note that these molecular frameworks are also representative of a high-mobility D−A conjugated polymer.[5b] Therefore, lessons learned by examina-

Chart 1. Chemical Structures of Fluorinated Molecules

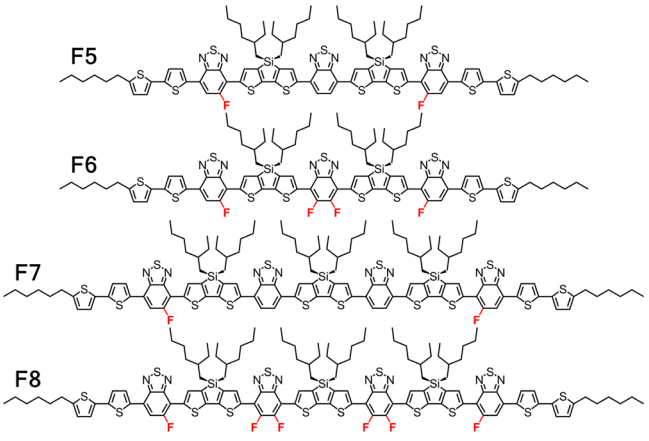

Received: September 30, 2014
Published: October 27, 2014

   dx.doi.org/10.1021/ja510088x | J. Am. Chem. Soc. 2014, 136, 16144−16147

Table 1. Optical, Electrochemical, and Thermal Transition Parameters of Molecules F5−F8

molecule	soln λ_{max} (nm)[a]	soln λ_{onset} (nm)[a]	film λ_{onset} (nm)[b]	E_g^{opt} (eV)[b]	E_{HOMO} (eV)[c]	E_{LUMO} (eV)[c]	E_g^{elec} (eV)[c]	T_m (°C)[d]	ΔH_m (J/g)[d]	T_c (°C)[d]	ΔH_c (J/g)[d]
F5	620	710	830	1.49	−5.2	−3.7	1.5	247	26.6	215	21.2
F6	618	700	805	1.54	−5.3	−3.7	1.6	279	29.2	253	27.0
F7	637	730	850	1.46	−5.1	−3.7	1.4	302	17.1	276	16.6
F8	627	715	800	1.55	−5.3	−3.7	1.6	322	6.9	287	6.5

[a]Measured in 0.02 mg/mL chloroform solutions. [b]Thin films were prepared by spin-coating chloroform solutions (10 mg/mL) atop glass slides. [c]Energy levels were determined from the onsets of the respective oxidation and reduction processes with respect to Fc/Fc^+ (−4.88 eV vs vacuum), and measured from drop-cast films on glassy carbon electrodes. [d]DSC measurements were carried out under N_2 atmosphere with a heating/cooling ramp of 10 °C/min. Enthalpies (melting: ΔH_m, crystallization: ΔH_c) were obtained by integrating each thermal transition peak.

tion of **F5−F8** are relevant within the context of materials classes implemented in optoelectronic technologies.

Molecules **F5−F8** were prepared from a series of microwave-assisted Stille coupling reactions.[11] Synthesis and characterization data can be found in the Supporting Information (SI). Chemical compositions were confirmed by using field desorption mass spectrometry and ^1H, ^{19}F, and ^{13}C nuclear magnetic resonance (NMR) spectroscopy in 1,1,2,2-tetrachloroethane-d_2 at 120 °C. It is worth noting from a practical perspective that fluorine substitution leads to a general decrease in solubility. Compounds **F5** and **F7**, with two fluorine atoms per molecule, can be dissolved in chloroform in excess of 25 mg/mL. For comparison, the tetrafluorinated **F6** and hexafluorinated **F8** are marginally soluble in chloroform (<5 mg/mL) at room temperature, while solutions with concentrations of 15−20 mg/mL can be obtained at temperatures >50 °C. The noticeable decrease in solubility (**F8** vs **F7**, **F6** vs **F5**) hints to an enhanced interchromophore association upon molecular fluorination.

Solution UV−vis absorption spectra reveal extinction coefficients (ε) at the absorption maxima (λ_{max}, Table 1) of 9.6 × 10^4, 1.04 × 10^5, 1.26 × 10^5, and 1.35 × 10^5 $M^{-1}\cdot cm^{-1}$ for **F5−F8**, respectively. Table 1 summarizes relevant molecular properties. The additional fluorination on **F5** or **F7** (i.e., **F6** or **F8**, respectively) leads to slightly higher ε values, together with emergence of vibronic-like features (Figure S1). Figure 1a shows

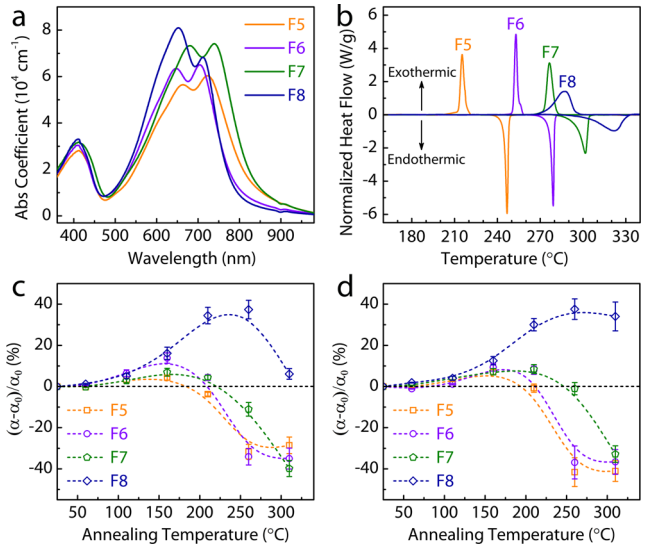

Figure 1. (a) UV−vis absorption profiles of **F5−F8** thin films. (b) DSC traces of the corresponding molecules (baseline correction was performed). Percentile changes of solid-state absorption coefficients of the lowest energy bands for each molecule as a function of annealing temperature under air (c) or N_2 atmosphere (d).

the absorption of **F5−F8** thin films casted onto precleaned glass slides from chloroform solutions (10 mg/mL). The 10 mg/mL solutions of **F6** and **F8** were achieved by heating at 50 °C and cooling to room temperature before thin-film preparation. Unlike molecules **F5−F7**, which exhibit stronger low-energy bands, only a weak shoulder peak at 705 nm is observed for **F8**. This feature may relate to a less precise molecular ordering.[12] Optical band gaps were estimated from the absorption onsets of thin films as (in eV) 1.49 (**F5**), 1.54 (**F6**), 1.46 (**F7**), and 1.55 (**F8**). The highest occupied molecular orbital (HOMO) and lowest unoccupied molecular orbital (LUMO) energy levels (E_{HOMO} and E_{LUMO}) were estimated from cyclic voltammetry measurements (Figure S2). Interestingly, E_{LUMO} (−3.7 eV) appears insensitive to either molecular length or fluorine substitution within this series of molecules, at least within the precision afforded by these electrochemical measurements. In contrast, E_{HOMO} appears to be more strongly perturbed by the degree of fluorine substitution, i.e., −5.3 eV (**F6**) vs −5.2 eV (**F5**) and −5.3 eV (**F8**) vs −5.1 eV (**F7**). The correlations between the number of fluorine atoms and the deepening in E_{HOMO} imply that a material with a higher degree of fluorination may be more resistant against oxidation. While molecular fluorination provides relatively minor modification of molecular-level properties, as discussed in more detail below, it has a significantly higher impact on the solid-state behavior, especially melting transitions.

Figure 1b provides the differential scanning calorimetry (DSC) traces of molecules **F5−F8** under equilibrated conditions. Melting (T_m) and crystallization (T_c) temperatures, together with the corresponding enthalpies (ΔH_m and ΔH_c) are listed in Table 1. Double C−H for C−F substitution on **F5** (i.e., **F6**) results in 32 and 38 °C increases in T_m and T_c, respectively, corroborating stronger intermolecular contacts in the bulk. A similar behavior is observed for **F8** vs **F7** (increases of 20 °C in T_m and 11 °C in T_c). The consistent trends suggest that a higher degree of fluorination achieves stronger intermolecular interactions, thus a higher thermal energy input is required to overcome such force and drive the material into a more isotropic state. A relative degree of crystallinity may be mapped out by comparing ΔH_m and ΔH_c between structurally related molecular analogues. Using the values from Table 1, for **F6** vs **F5**, one observes increases in ΔH_m and ΔH_c of 2.6 and 5.8 J/g, respectively. Instead, **F8** shows decreases in ΔH_m and ΔH_c of more than 10 J/g as compared with **F7**.

For conjugated polymers and molecules, the lowest energy peak in the absorption spectrum is often indicative of structural ordering in the material bulk.[12b] Changes in such features as a function of thermal treatment can be quantified by comparing the film absorption coefficient (α) after heating with the value obtained from as-cast films (α_0). Figure 1c,d shows plots of $(\alpha - \alpha_0)/\alpha_0$ vs annealing temperature (T_a) under air or nitrogen,

dx.doi.org/10.1021/ja510088x | J. Am. Chem. Soc. 2014, 136, 16144−16147

respectively. Molecules **F5**−**F7** show <10% increase in α with T_a < 200 °C both under air and N_2, pointing to thermally resistant optical features and bulk morphology. Decreases in $(\alpha - \alpha_0)/\alpha_0$ for **F5**−**F7** between 200 and 250 °C at T_a rank in the order of **F5** < **F6** < **F7**. This result is in agreement with the T_m values observed in the DSC experiments. In contrast, the low-energy absorption peak at 720 nm increases for **F8** when $T_a \leq 260$ °C under air, with an increase in α over α_0 of over 40%. Presumably, the larger size of **F8** makes it difficult for molecules to organize directly from solution, and subsequent heating promotes order within the thin film. When $T_a > 260$ °C, an obvious drop in the α of **F8** is observed. However, under an O_2-free environment, the **F8** film is able to sustain at $T_a = 310$ °C an α value that is ∼40% over α_0. This set of data suggests the initial drop in α for **F8** in air is most reasonably due to oxidation.

FET devices were employed to evaluate the T_a dependence of charge transport. Devices were fabricated with a bottom-gate top-contact geometry (SI). Thin films were casted from chloroform solutions of **F5**−**F8** (4 mg/mL) onto heavily doped silicon substrates with 300 nm of passivated silicon dioxide. Devices were postannealed under N_2 successively at various temperatures for 2 min for the T_a-dependent hole mobility (μ) studies. Figure 2a summarizes the data obtained for

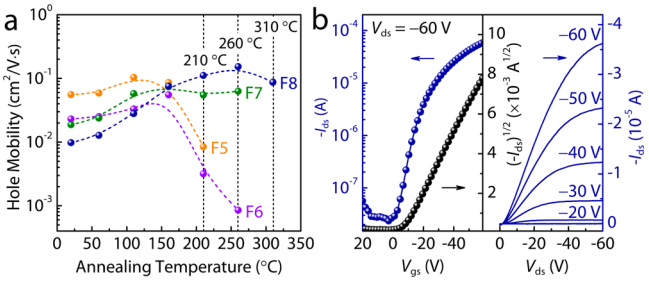

Figure 2. (a) Field-effect hole mobility as a function of annealing temperature for molecules **F5**−**F8**. (b) Transfer and output characteristics for **F8** device after thermal annealed at 310 °C for 2 min.

μ vs T_a. Initial thermal annealing (T_a < 110 °C) provides an increase of μ for all molecules. The T_a where the highest μ obtained is 110 °C for **F5**, 160 °C for **F6** and **F7**, and 260 °C for **F8**. Figure 2b shows transfer and output characteristics of **F8** device at $T_a = 310$ °C, $-I_{ds}$ vs V_{gs} (ds = drain source, and gs = gate source), $(-I_{ds})^{1/2}$ vs V_{gs} at $V_{ds} = -60$ V, and $-I_{ds}$ vs V_{ds} at V_{gs} from 0 to −60 V. *Most remarkably*, the **F8** device is able to retain its FET function upon thermal treatment to 310 °C, showing a μ = 0.09 cm^2/V·s, a threshold voltage of −10 V, and an on/off ratio of >10^3.

The positive effect of molecular elongation (**F7**, **F8** vs **F5**, **F6**) on FET thermal stability is consistent with previous reports.[10a] Moreover, the highest temperature sustainable before losing transistor function correlates positively with the degree of fluorination. Although the **F6** device shows a generally lower μ than that of **F5**, for the temperature windows studied herein, the **F6** device can survive at $T_a = 260$ °C, while the **F5** device fails beyond $T_a = 210$ °C. The same trend was observed for **F8** vs **F7**, for which devices function at $T_a = 310$ and 260 °C, respectively. These observations agree with the results from T_a-dependent optical properties (Figure 1d), in which molecules with longer dimension and higher degree of fluorination can maintain bulk textures at higher T_a.

The internal molecular order within the films upon thermal treatment was studied by using grazing incidence X-ray diffraction (GIXRD).[13] Incidence angles were chosen using X-ray reflectivity measurements to maximize diffraction signals (Figure S5). For T_a-dependent experiments, the same thin film was treated successively at different temperatures for 2 min, followed by quenching to room temperature. Out-of-plane and in-plane scans at different T_a can be found in Figure S6. Examination of the GIXRD traces reveals that **F5**−**F8** films exhibit strong (100) peaks preferentially along the out-of-plane direction and (010) peaks along the in-plane direction. These observations suggest that the direction of interchromophore π−π stacking of **F5**−**F8** molecules is predominantly perpendicular to the silicon surface normal, also known as "edge-on" orientation. Both *d*-spacing and crystallite coherence length (L_c) were extracted from fitting the "lamellar" and π-stacking diffraction peaks (SI). As shown in Figure 3a, the lamellar *d*-spacing for as-

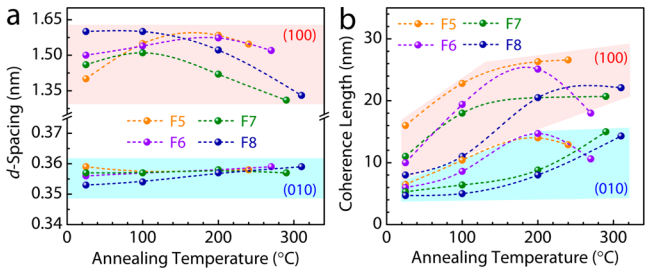

Figure 3. *d*-Spacing (a) and coherence length (b) from both out-of-plane (100) and in-plane (010) diffractions as a function of annealing temperature for films of **F5**−**F8** atop (100) silicon substrates.

cast films varies in the range from 1.3 to 1.6 nm in the order: **F5** < **F6** < **F7** < **F8**. Under the same as-cast conditions, π-stacking *d*-spacings for **F6** (3.56 Å) and **F8** (3.53 Å) were observed to be smaller than for **F5** (3.59 Å) and **F7** (3.57 Å), respectively, consistent with previous observations that fluorinated molecules, e.g., pentacene derivatives, show a closer π−π interplanar distance than for nonfluorinated ones.[14] Figure 3b shows L_c as a function of T_a. L_c values along the (100) direction, denoted as $L_{c\,(100)}$, reach 15−25 nm for **F5**−**F8** as T_a approaches T_m. **F5** and **F6** show a maximum $L_{c\,(010)}$ of ∼15 nm near $T_a = 200$ °C, while $L_{c\,(010)}$ of **F7** and **F8** increases even with T_a close to T_m. It is worth noting that **F8** film shows $L_{c\,(100)} = 22$ nm and $L_{c\,(010)} = 14$ nm at $T_a = 310$ °C, implying a robust crystalline bulk toward extreme conditions. The current set of experiments corroborates that molecular fluorination of these D−A oligomers can effectively preserve crystallite thermal stability, leading to notable charge carrier mobilities toward higher T_a, which is likely due to additional intermolecular F···S, F···H, and F···π interactions.[3]

The T_m of 322 °C of **F8** is among the highest values reported for solution-processable conjugated small molecules (e.g., 6,13-bis(triisopropylsilylethynyl)pentacene), oligomers and even polymers (molecular weight >20 kDa).[15] It is worth pointing out here that the T_m of **F8** also approaches the values of those processable only from their solid states, e.g., tetracene, pentacene, and rubrene.[16] With the current molecular design protocol, it is possible for one to synthesize molecular materials with a combination of high T_m, solution processability, and thermally stable bulk morphology, which may open a door to versatile processing conditions with reliable device performances.

In conclusion, four donor−acceptor molecules with different lengths and different numbers of fluorine substitutions were synthesized with the aim to study the effect of molecular

dx.doi.org/10.1021/ja510088x | J. Am. Chem. Soc. 2014, 136, 16144−16147

fluorination on bulk thermal properties relevant to organic semiconducting device applications. We have shown that remarkably robust bulk textures may be achieved by virtue of molecules with intermediate dimensions and a higher degree of fluorination. When fabricated in thin-film FET devices, longer molecular length and higher degrees of fluorination promote a more thermally resistant bulk organization for charge transport function. These findings are particularly important when considering high-temperature processing, organic−inorganic hybrid materials, and long-term device durability under extreme environmental conditions.

■ ASSOCIATED CONTENT

Supporting Information

Synthesis and optical properties of **F5**−**F8**. Electrochemical characterizations. Annealing temperature-dependent optical properties of thin films under both ambient and inert conditions. XRR curves and films thickness calculation. GIXRD profiles of thin films before and after thermal annealing at various temperatures. OFET device fabrication and testing. This material is available free of charge via the Internet at http://pubs.acs.org.

■ AUTHOR INFORMATION

Corresponding Author

bazan@chem.ucsb.edu

Notes

The authors declare no competing financial interest.

■ ACKNOWLEDGMENTS

The synthesis work was supported by the Office of Naval Research (N00014-14-1-0101) and the characterization work by the Institute of Collaborative Biotechnology through grant W911NF-09-0001 from the U.S. Army Research Office. Financial support for device testing was by National Science Foundation (DMR 0856060) and Department of Energy, Office of Basic Energy Sciences under award no. DE-FG02-08ER46535. X.L. thanks Prof. Michael L. Chabinyc and Dr. Louis A. Perez for helpful discussion on X-ray characterization.

■ REFERENCES

(1) (a) Liang, T.; Neumann, C. N.; Ritter, T. *Angew. Chem., Int. Ed.* **2013**, *52*, 8214−8264. (b) O'Hagan, D. *Chem. Soc. Rev.* **2008**, *37*, 308−319. (c) Sperati, C. A.; Starkweather, H. W., Jr. In *Fortschritte Der Hochpolymeren-Forschung*; Springer: Berlin Heidelberg, 1961; Vol. *2/4*, pp 465−495.

(2) (a) Babudri, F.; Farinola, G. M.; Naso, F.; Ragni, R. *Chem. Commun.* **2007**, 1003−1022. (b) Katz, H. E.; Lovinger, A. J.; Johnson, J.; Kloc, C.; Siegrist, T.; Li, W.; Lin, Y. Y.; Dodabalapur, A. *Nature* **2000**, *404*, 478−481. (c) Sakamoto, Y.; Komatsu, S.; Suzuki, T. *J. Am. Chem. Soc.* **2001**, *123*, 4643−4644. (d) Renak, M. L.; Bartholomew, G. P.; Wang, S.; Ricatto, P. J.; Lachicotte, R. J.; Bazan, G. C. *J. Am. Chem. Soc.* **1999**, *121*, 7787−7799.

(3) Reichenbacher, K.; Suss, H. I.; Hulliger, J. *Chem. Soc. Rev.* **2005**, *34*, 22−30.

(4) (a) Tumbleston, J. R.; Stuart, A. C.; Gann, E.; You, W.; Ade, H. *Adv. Funct. Mater.* **2013**, *23*, 3463−3470. (b) Son, H. J.; Wang, W.; Xu, T.; Liang, Y.; Wu, Y.; Li, G.; Yu, L. *J. Am. Chem. Soc.* **2011**, *133*, 1885−1894. (c) van der Poll, T. S.; Love, J. A.; Nguyen, T. Q.; Bazan, G. C. *Adv. Mater.* **2012**, *24*, 3646−3649. (d) Bronstein, H.; Frost, J. M.; Hadipour, A.; Kim, Y.; Nielsen, C. B.; Ashraf, R. S.; Rand, B. P.; Watkins, S.; McCulloch, I. *Chem. Mater.* **2013**, *25*, 277−285. (e) You, J.; Dou, L.; Yoshimura, K.; Kato, T.; Ohya, K.; Moriarty, T.; Emery, K.; Chen, C. C.; Gao, J.; Li, G.; Yang, Y. *Nat. Commun.* **2013**, *4*, 1446. (f) Tumbleston, J. R.; Collins, B. A.; Yang, L.; Stuart, A. C.; Gann, E.; Ma, W.; You, W.; Ade, H. *Nat. Photonics* **2014**, *8*, 385−391. (g) Stuart, A. C.; Tumbleston, J. R.; Zhou, H.; Li, W.; Liu, S.; Ade, H.; You, W. *J. Am. Chem. Soc.* **2013**, *135*, 1806−1815.

(5) (a) Yuan, Y.; Giri, G.; Ayzner, A. L.; Zoombelt, A. P.; Mannsfeld, S. C.; Chen, J.; Nordlund, D.; Toney, M. F.; Huang, J.; Bao, Z. *Nat. Commun.* **2014**, *5*, 3005. (b) Luo, C.; Kyaw, A. K.; Perez, L. A.; Patel, S.; Wang, M.; Grimm, B.; Bazan, G. C.; Kramer, E. J.; Heeger, A. J. *Nano Lett.* **2014**, *14*, 2764−2771.

(6) (a) Liu, H.; Xu, J.; Li, Y.; Li, Y. *Acc. Chem. Res.* **2010**, *43*, 1496−1508. (b) Li, Y.; Liu, T.; Liu, H.; Tian, M. Z.; Li, Y. *Acc. Chem. Res.* **2014**, *47*, 1186−1198.

(7) (a) Cho, S.; Seo, J. H.; Park, S. H.; Beaupre, S.; Leclerc, M.; Heeger, A. J. *Adv. Mater.* **2010**, *22*, 1253−1257. (b) Treat, N. D.; Shuttle, C. G.; Toney, M. F.; Hawker, C. J.; Chabinyc, M. L. *J. Mater. Chem.* **2011**, *21*, 15224−15231. (c) Lindqvist, C.; Bergqvist, J.; Feng, C.-C.; Gustafsson, S.; Bäcke, O.; Treat, N. D.; Bounioux, C.; Henriksson, P.; Kroon, R.; Wang, E.; Sanz-Velasco, A.; Kristiansen, P. M.; Stingelin, N.; Olsson, E.; Inganäs, O.; Andersson, M. R.; Müller, C. *Adv. Energy Mater.* **2014**, DOI: 10.1002/aenm.201301437. (d) Liao, M.-H.; Tsai, C.-E.; Lai, Y.-Y.; Cao, F.-Y.; Wu, J.-S.; Wang, C.-L.; Hsu, C.-S.; Liau, I.; Cheng, Y.-J. *Adv. Funct. Mater.* **2014**, *24*, 1418−1429. (e) Kim, B. J.; Miyamoto, Y.; Ma, B.; Fréchet, J. M. J. *Adv. Funct. Mater.* **2009**, *19*, 2273−2281.

(8) Subramanian, S.; Park, S. K.; Parkin, S. R.; Podzorov, V.; Jackson, T. N.; Anthony, J. E. *J. Am. Chem. Soc.* **2008**, *130*, 2706−2707.

(9) (a) Krebs, F. C.; Fyenbo, J.; Jørgensen, M. *J. Mater. Chem.* **2010**, *20*, 8994−9001. (b) Green, R.; Morfa, A.; Ferguson, A. J.; Kopidakis, N.; Rumbles, G.; Shaheen, S. E. *Appl. Phys. Lett.* **2008**, *92*, 033301. (c) Perelaer, J.; Abbel, R.; Wunscher, S.; Jani, R.; van Lammeren, T.; Schubert, U. S. *Adv. Mater.* **2012**, *24*, 2620−2625.

(10) (a) Liu, X.; Sun, Y.; Perez, L. A.; Wen, W.; Toney, M. F.; Heeger, A. J.; Bazan, G. C. *J. Am. Chem. Soc.* **2012**, *134*, 20609−20612. (b) Liu, X.; Sun, Y.; Hsu, B. B.; Lorbach, A.; Qi, L.; Heeger, A. J.; Bazan, G. C. *J. Am. Chem. Soc.* **2014**, *136*, 5697−5708.

(11) Carsten, B.; He, F.; Son, H. J.; Xu, T.; Yu, L. *Chem. Rev.* **2011**, *111*, 1493−1528.

(12) (a) Park, Y. D.; Park, J. K.; Seo, J. H.; Yuen, J. D.; Lee, W. H.; Cho, K.; Bazan, G. C. *Adv. Energy Mater.* **2011**, *1*, 63−67. (b) Peet, J.; Kim, J. Y.; Coates, N. E.; Ma, W. L.; Moses, D.; Heeger, A. J.; Bazan, G. C. *Nat. Mater.* **2007**, *6*, 497−500.

(13) (a) Widjonarko, N. E.; Schulz, P.; Parilla, P. A.; Perkins, C. L.; Ndione, P. F.; Sigdel, A. K.; Olson, D. C.; Ginley, D. S.; Kahn, A.; Toney, M. F.; Berry, J. J. *Adv. Energy Mater.* **2014**, DOI: 10.1002/aenm.201301879. (b) Rivnay, J.; Mannsfeld, S. C.; Miller, C. E.; Salleo, A.; Toney, M. F. *Chem. Rev.* **2012**, *112*, 5488−5519. (c) Chabinyc, M. L. *Polym. Rev.* **2008**, *48*, 463−492.

(14) (a) Sakamoto, Y.; Suzuki, T.; Kobayashi, M.; Gao, Y.; Fukai, Y.; Inoue, Y.; Sato, F.; Tokito, S. *J. Am. Chem. Soc.* **2004**, *126*, 8138−8140. (b) Swartz, C. R.; Parkin, S. R.; Bullock, J. E.; Anthony, J. E.; Mayer, A. C.; Malliaras, G. G. *Org. Lett.* **2005**, *7*, 3163−3166.

(15) (a) Mitsui, C.; Okamoto, T.; Yamagishi, M.; Tsurumi, J.; Yoshimoto, K.; Nakahara, K.; Soeda, J.; Hirose, Y.; Sato, H.; Yamano, A.; Uemura, T.; Takeya, J. *Adv. Mater.* **2014**, *26*, 4546−4551. (b) Usta, H.; Risko, C.; Wang, Z.; Huang, H.; Deliomeroglu, M. K.; Zhukhovitskiy, A.; Facchetti, A.; Marks, T. J. *J. Am. Chem. Soc.* **2009**, *131*, 5586−5608. (c) Nishide, Y.; Osuga, H.; Saito, M.; Aiba, T.; Inagaki, Y.; Doge, Y.; Tanaka, K. *J. Org. Chem.* **2007**, *72*, 9141−9151. (d) Baklar, M.; Barard, S.; Sparrowe, D.; Wilson, R. M.; McCulloch, I.; Heeney, M.; Kreouzis, T.; Stingelin, N. *Polym. Chem.* **2010**, *1*, 1448−1452. (e) Guo, X.; Zhou, N.; Lou, S. J.; Smith, J.; Tice, D. B.; Hennek, J. W.; Ortiz, R. P.; Navarrete, J. T. L.; Li, S.; Strzalka, J.; Chen, L. X.; Chang, R. P. H.; Facchetti, A.; Marks, T. J. *Nat. Photonics* **2013**, *7*, 825−833. (f) Ahmed, E.; Ren, G. Q.; Kim, F. S.; Hollenbeck, E. C.; Jenekhe, S. A. *Chem. Mater.* **2011**, *23*, 4563−4577. (g) Li, Z.; Lu, J. P.; Tse, S. C.; Zhou, J. Y.; Du, X. M.; Tao, Y.; Ding, J. F. *J. Mater. Chem.* **2011**, *21*, 3226−3233.

(16) Baklar, M. A.; Koch, F.; Kumar, A.; Domingo, E. B.; Campoy-Quiles, M.; Feldman, K.; Yu, L.; Wobkenberg, P.; Ball, J.; Wilson, R. M.; McCulloch, I.; Kreouzis, T.; Heeney, M.; Anthopoulos, T.; Smith, P.; Stingelin, N. *Adv. Mater.* **2010**, *22*, 3942−3947.